Voltage and frequency controlled Ge/SeO$_2$ thin film transistors designed as rectifiers, negative capacitance and negative conductance sources

A. F. Qasrawi [a,c,*] ,   Hazem K. Khanfar[b]
[a]Department of Physics, Arab American University, Jenin, Palestine
[b]Department of Telecommunication Engineering, Arab American University, Jenin 240, Palestine
[c]Department of Electrical and Electronics Engineering, Istinye University, 34010, Istanbul, Turkey

Herein voltage and frequency controlled thin film transistors fabricated by depositing SeO$_2$ onto germanium thin crystals are reported. For these devices measurements of the current-voltage characteristics revealed a biasing dependent rectification ratios. The devices showed metal-oxide-semiconductor character under reverse biasing conditions. In addition, the biasing dependent capacitance and conductance spectral studies in the frequency domain of 20M-1000MHz has shown the possibility of switching the capacitance and negative conductance from negative mode to positive mode. The features of the Ge/SeO$_2$ devices make them attractive for use in electronic circuits as parasitic capacitive circuit elements, noise reducers, signal amplifiers and microwave oscillators.

1. Introduction

Germanium substrates are in focus of research society due to their wide range of applications in technological industry. These substrates are mentioned suitable for fabrication of high efficiency multi-junction solar cells due to their excellent infrared sensitivity in the spectral range of 750-1900 nm [1]. Germanium substrates are also employed for fabricating NiGe low noise metal oxide field effect transistors (MOSFET) [2]. The NiGe/n-Ge(100) Schottky barrier diodes as MOSFETs are nominated for low leakage Ge-MOSFET applications [2]. In addition, coating germanium substrates with metal oxide layers are reported enhancing the electrical performance of capacitors through formation of oxide layer at the ultrathin interface [3, 4]. One of the oxides that are rarely studied as member of electronic technology is selenium oxide. This material is highly transparent and exhibit wide energy band gap of 3.69-3.77 eV [5, 6, 7]. SeO$_2$ coated onto Ag substrates is observed showing negative capacitance and negative conductance effects [6, 7]. These two features are attractive for signal amplification and noise reduction in thin film transistors. Thus coating SeO$_2$ onto Ge is promising because they indicate formation of narrow/wide gap heterojunctions suitable for multi-functional operations. In truth the narrow energy band gap of Ge (0.68 eV) and the high electron mobility in addition to the light effective mass [4] makes it favorable for us to use it as substrates to grow SeO$_2$ thin films to form germanium/metal oxide interfaces.   For this reason, here in this work we will grow selenium oxide thin films onto thin crystals of cubic germanium and study their structural and electrical properties. We are showing that Ge/SeO$_2$ interfaces can perform as high frequency MOS transistors responsive in the microwave frequency domain. We will also show that the proposed devices can be easily controlled by the applied voltage to engineer the negativity of the conductance and capacitance. The possible applications of the Ge/SeO$_2$ interface will also be suggested.

---

* Corresponding author: atef.qasrawi@aaup.edu

2. Experimental details

Thin germanium crystals (Alpha Aeser, 99.99%) of sizes of $0.3 \times 0.3 \times 0.10$ cm^3 are used as substrates to deposit selenium oxide thin films of thicknesses of 1.0 μm. The SeO$_2$ films and Ge crystal surfaces are coated with Ag metal to form metal contacts using appropriate masks. In the fabrication process, selenium oxide powders (Alpha Aeser, 99.90%) are used to prepare thin films using VCM-600 thermal evaporator. The vacuum pressure was kept ~10^{-5} mbar. The thickness of the samples was measured via SOLID IN II profile-meter capable of measuring thicknesses in the range of 5.0 nm-1000 μm. The crystal structure was explored by Miniflex 600 X-ray diffraction unit running at scanning speed of 0.1°/min. The surface morphology and compositional stoichiometry were studied using COXEM 200 scanning electron microscope equipped with EDAX energy dispersive X-ray analyzer. The current-voltage characteristics were measured using an automated Keithley $I - V$ system comprising Keithley 230 Voltage source and Keithley 6485 Picoammeter. The automation is made via IEEE-488 card and Matlab software packages. The impedance spectroscopy was recorded with Agilent 4291B 10-1800 MHz impedance analyzer. The $n-$Ge and p- SeO$_2$ conductivity type of the samples was measured using the hot probe technique.

3. Results and discussion

In this work we propose Ge based new class of heterojunction devices. The selected oxide layer is SeO$_2$. The schematics for the Ge/SeO$_2$ stacked layers are shown in the inset of Fig. 1 (a). Fig. 1(a) additionally illustrates the X-ray diffraction (XRD) patterns for Ge crystals and Ge/SeO$_2$ heterojunctions.
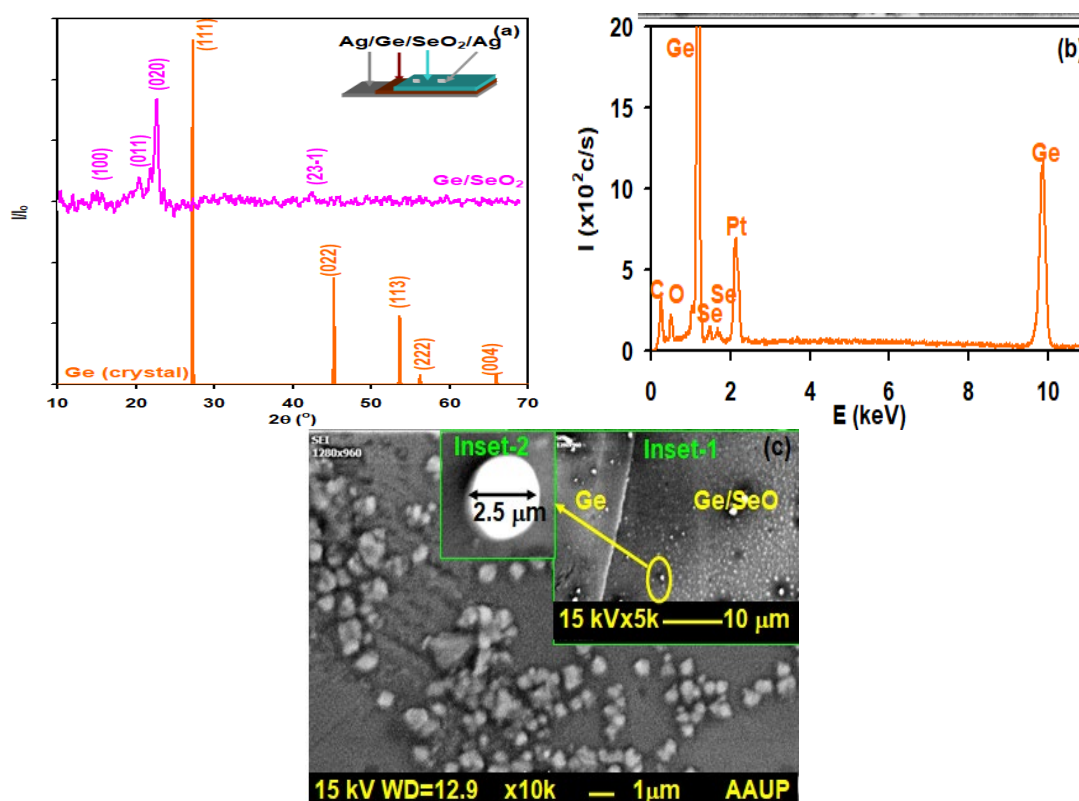
Fig. 1. (a) the X-ray diffraction patterns and (b) the energy dispersive X-ray spectra for SeO$_2$ films coated onto Ge crystals. (c) A scanning electron microscopy image taken for SeO$_2$ coated onto Ge. The inset of (a) showing the schematics of the geometrical design, inset-1 of (c) displaying the interface region. Inset-2 of (c) is an enlargement of the circular grains observed at the Ge/SeO$_2$ interfaces.

The sharp patterns which appear in the figure are analyzed using "Crystdiff" software packages. While Ge crystals display peaks that are assigned to cubic Ge of lattice parameters of $a = b = c = 5.65$ Å (JCPDS card No. 03-065-0333), SeO_2 display sharp patterns relating to tetragonal SeO_2 with lattice parameters of $a = b = 7.89$ Å, $c = 5.60$ Å and space group of P_{4222} [6, 7]. The lattice mismatches between Ge and SeO_2 along the c −axis is $\Delta\% = \frac{|c_{SeO2}-c_{Ge}|}{c_{SeO2}}.100=$ 0.89%. The lattice mismatches along the a- and b −axis are ~151.6%. It is clear from the numerical data that the substrate (Ge) and epilayer (SeO_2) are well aligned along the c −axis and highly mismatched along the a −and b −axes. This property makes electronic transport along the c −axis much easier than along the other axes. It was observed that the smaller the lattice mismatches, the higher the electrical conductivity [8].

Fig. 1 (b) illustrates the energy dispersive X-ray spectra (EDS) for the Ge/SeO_2 interfaces. The spectra indicate the presence of Ge, Se, O, C and Pt atoms only. No other impurities were detected. Pt appears because the samples were coated with Pt to prevent electron contaminations. The carbon peak is due to carbon the contact band which is used to guarantee well contacts between the sample and the sample holder in the microscope. The atomic content analysis indicated that selenium oxide is composed of 34.91 at. % Se and 65.09 at.% O. The corresponding chemical formula is $SeO_{1.86}$. It is clear that SeO_2 is oxygen deficient. That is some oxygen vacancies do exist in the SeO_2 films. Oxygen vacancies can result in high leakage currents in devices [9]. In addition, inset-1 of Fig. 1 (c) show the scanning electron microscopy (SEM) images for the interface region. Enlargement of 5000 times shows that the interface boundary is straight and sharp indicating the uniform formation of the Ge/SeO_2 interfaces. Generally, the epilayer (SeO_2) layer is composed of two types of grains. The grains are shown in Fig. 1 (c). Most of the grains are irregular or rectangular shaped and display an average size of 850 nm. Some rarely observed disk like grains which are shown in inset-2 of Fig. 1 (c) display diameter of 2.5 μm.

The energy band diagram for the Ge/SeO_2 interfaces is illustrated in Fig. 2 (a). In accordance with the diagram, the built in potential ($qV_{bi} = |q\phi_2 - q\phi_1|$), work function of n −Ge ($q\phi_1$) and of p −SeO_2 are 1.11 eV, 4.37 eV [10] and 5.48 eV [6], respectively.
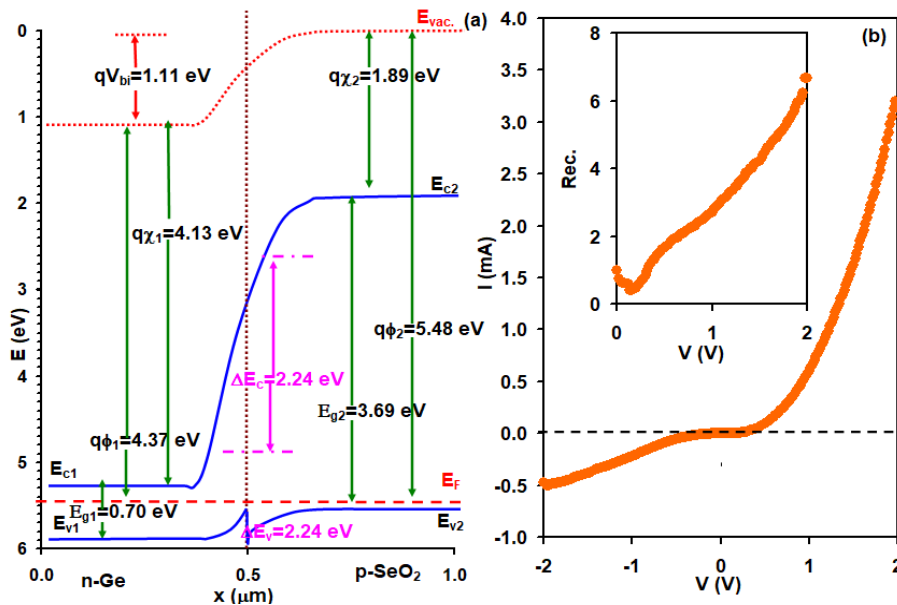
Fig. 2. (a) the energy band diagram and (b) the current-voltage characteristics being collected between the gate and source of the AGSA devices. The inset of (b) showing the biasing dependent current rectification ratios.

The band bending mechanism indicates lowering of the vacuum level of $n-$region to allow alignment of Fermi levels (E_F). The relatively large built in potential originate from using wide band gap SeO$_2$. SeO$_2$ is observed exhibiting energy band gap of 3.69 eV [7].In addition, the conduction and valence bands offsets are $\Delta E_c = |q\chi_1 - q\chi_2|$=2.24 eV and $\Delta E_v = |(E_{g2} - E_{g1}) - \Delta E_c| = 0.75$ eV. The values are sufficiently large to prevent electron hole recombination at the Ge/SeO$_2$ interfaces [11]. On the other hand, since the work function of face centered cubic Ag metal is 4.74 eV [12], then Ag/$n-$Ge and Ag/$p-$SeO$_2$ form Schottky barriers of $qV_{bi} = |q\phi_{Ag} - q\phi_{n-Ge}|$= 0.37 eV and $qV_{bi} = |q\phi_{Ag} - q\phi_{p-SeO2}|$= 0.74 eV, respectively. Hence, the proposed Ag/$p-$Ge/$p-$SeO$_2$/Ag (AGSA) device is hybrid device composed of $n-$Schttky, pn junction and $p-$Schottky. The sum of the flat band built in potentials of the device can reach 2.22 eV.

The current (I)-voltage (V) characteristics for the AGSA devices is shown in Fig. 2 (b). The positive applied voltage (forward biasing) was connected to the Ag/$p-$SeO$_2$ arm. In general, the current under forward biasing conditions is higher than that under reverse current. The current rectification ratios ($Rec. = I_{Forward}/I_{Reverse}$) increases with increasing biasing voltage (Inset of Fig. 2 (b)). The reverse biasing of the device reveals large leakage current. Large leakage current results from oxygen vacancies [13] (the currently studied films are oxygen deficient (EDS analyses)), small energy band gap of germanium at the Ag/$n-$Ge interface [14] and surface roughness [15]. The biasing dependence of rectification ratios also indicates the possible existence of electric field assisted tunneling processes [16]. Tunneling may not be dominant conduction mechanism by partially assisting the thermionic emission process [11]. Our attempts to explore the dominant current conduction mechanism in AGSA devices included Richardson Schottky type of conduction followed by Cheung's functional analysis in which the current is given by the relations [11, 17],

$$I = AA^*T^2 e^{-q\phi_B/kT}(e^{q(V-IR_s)/nkT} - 1),\tag{1}$$

$$\frac{dV}{dln(I)} = IR_s + n(\frac{kT}{q}),\tag{2}$$

and

$$H(I) = V - n\left(\frac{kT}{q}\right)\ln\left(\frac{I}{AA^*T^2}\right) = IR_s + nq\phi_B.\tag{3}$$

Here, $T = 300$ K, n is the ideality factor, R_s is the series resistance, $q\phi_B$ is the effective barrier height, $A = 0.0314\ cm^2$ is the diode area, $A^* = 120 m^*_{Ge/SeO2}$ =7.97 A/cm^{2}K^2 is the Richardson constant, $m^*_{Ge/SeO2}$ =$(m^{-1}_{e-Ge} + m^{-1}_{h-SeO2})^{-1} = 0.066 m_o$ (m^*_{e-Ge}=0.082m_o [18], m^*_{h-SeO2}=0.35m_o [7]) is the reduced effective mass, $H(I)$ is the Cheung's function [17]. Sketching the $\ln(I) - V$ variations which appear in Fig .3 (a) and finding the derivative ($dV/dln(I)$) and drawing it as function of I permit determining the ideality factor (n) after reduction of the series resistance effect. Thereafter, substituting the intercept value ($n\left(\frac{kT}{q}\right)$) which is determined from the $\frac{dV}{dln(I)} - I$ variations into Eqn. (3) allows calculating the value of the barrier height and series resistance. The plots of $\ln(I) - V$ (Fig. 3 (a)) discarding the series resistance ($R_s = 0\ \Omega$) effect results in n and $q\phi_B$ values of 2.94 and 2.77 and 0.66 eV and 0.65 eV for the diodes under forward and reverse conditions respectively. However, when the series resistance effect is taken into account by handling Cheung's analyses, Fig. 3 (b), the ideality factor and barrier height are found to be 2.05 and 1.19, 0.68 eV and 0.76 eV and the series resistance are 1.37 $k\Omega$ and 1.79 $k\Omega$ under forward and reverse biasing conditions, respectively. The deviation of the ideality factor from unity is additionally (other than series resistance effect) attributed to the, tunneling, drifts and diffusion effects in the depletion layer in addition to the high injection effects as well [11, 17].

It is also worth noting that analyses of the $I - V$ characteristics assuming the domination of electric field assisted tunneling presented by the equation [11, 16],

$$I = AA^{**}T^2V^\gamma\exp(-\frac{e\Phi}{kT})$$

(4)

$$\Phi = \phi_o - n\sqrt{e\eta/(4\pi\varepsilon_o\varepsilon_r)}\ \sqrt{V}/\sqrt{w}\ .$$

(5)

where, Φ is the electric field-dependent activation energy that represents a Schottky-barrier height in the presence of the electric field, $q\phi_o \equiv q\phi_b$ is the field independent value. For Schottky-Richardson field emission (tunneling) mechanism to dominate, the ideality factor $n = \eta = 1.0$ and $\gamma = 0$ is substituted. The linear fitting of the $\ln(I)$-$\sqrt{V}$ which is illustrated in Fig. 3 (c) reveal barrier heights and widths of 0.74 eV, 0.67 eV and 61 nm and 86 nm for forward and reverse biased currents, respectively. These calculations which were carried out assuming high frequency dielectric constants of 1.6 and 16.0 for SeO_2 [7] and Ge [18], respectively, also assure the possible domination of the tunneling mechanism in the samples. Hence we can conclude that the current conduction mechanism in AGSA devices is dominated by thermionic and tunneling process at the same time.
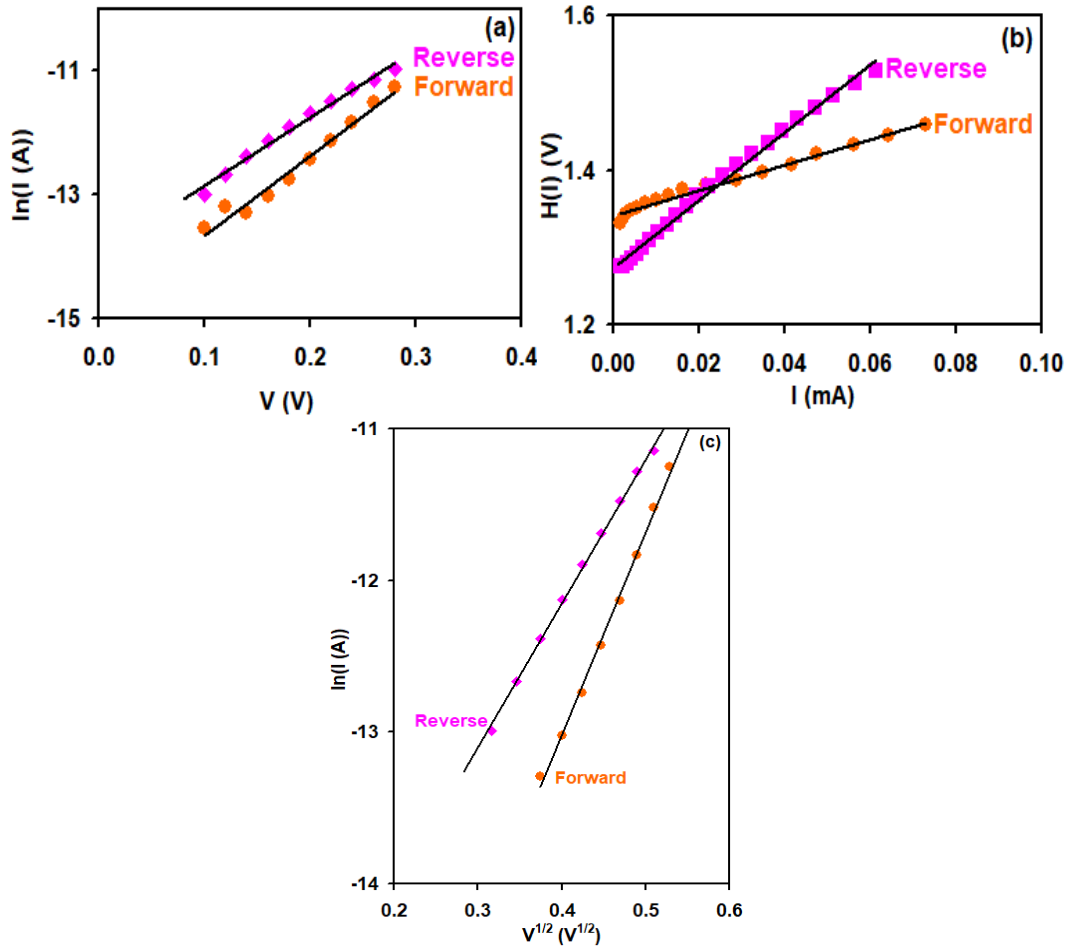
Fig. 3. (a) the $\ln(I) - V$ variations and (b) the Cheung's function plotting and (c) the $\ln(I) - \sqrt{V}$ variations for Ag/Ge/SeO₂/Ag devices

In order to explore the ability of the AGSA transistors to perform as metal-oxide-semiconductor (MOS) devices, the dc capacitance (C)-voltage characteristics are recorded in the frequency domain of 20-600 MHz. The amplitude of the ac signal was 0.10 V. The resulting

$C - V$ curves are shown in Fig. 4 (a) and (b). It is evident from the figures that the MOS device remains in the low capacitance mode when the devices are forward biased. For these devices, the surface potential increases to a point where the electron density at the surface equals the background ion density. At this point, the depletion region stops growing and the extra charge are provided by the inversion charge at the surface. The threshold voltages are defined as the gate-body voltage that causes the surface to change from p-type to n-type. For this condition, the surface potential has to equal the negative of the p-type potential. In reference with our figures shown in Fig. 4 (a) and (b), the device is depleted when reverse biased and reaches the inversion mode at particular voltage (-1.56 V) that is independent of the imposed signal frequency. Forward biasing the device keep it in the accumulation mode. Analyzing the depletion mode of the device in the frequency domain of 20- 100 MHz, assuming the validity of the abrupt approach for depleted capacitance was possible with the equation [11],

$$C^{-2} = \frac{2(V_{bi} - V - \frac{2kT}{q})}{q \varepsilon_r N} .$$

(5)

The slope and intercepts of the linear plots of the $C^{-2} - V$ variations which are illustrated in Fig. 4 (c) allows calculation of qV_{bi} and the free charge carrier density (N) which are illustrated in Fig. 4 (d). It is clear from the figure that the built in potential increases with increasing signal frequency reaching value of 1.72 eV at 100 MHz. The values of the built in potentials are less than we theoretically estimated for flat band calculations (Fig. 2 (a)). It is also obvious from Fig. 4 (d) that the free charge carrier density decreases with increasing signal frequency in the frequency domain of 20-50 MHz. It tends to remain constant for higher applied signal frequencies. The increase in V_{bi} values that is associated with decrease in free Carrier density values with increasing signal frequency can be assigned to the inability of the free charge carriers to orient with oscillatory incident electric signals [19].
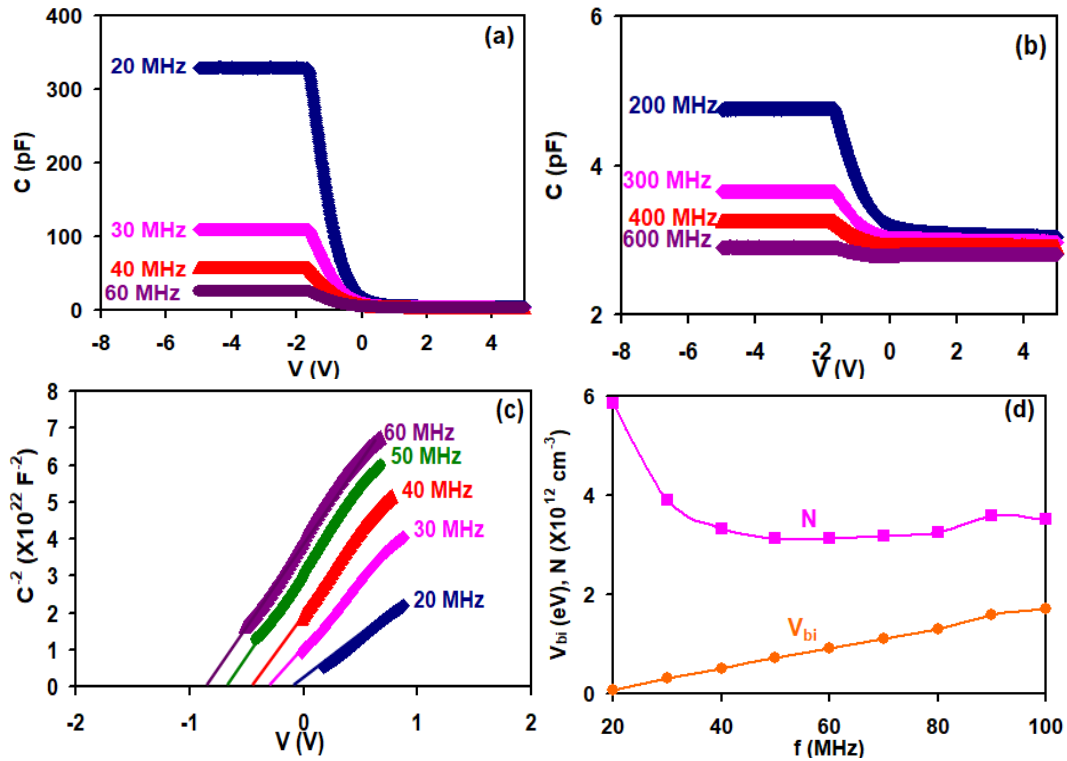
Fig. 4. The capacitance- voltage characteristics in the frequency ranges of (a) 20-60 MHz and (b) 200-600 MHz. (c) the $C^{-2} - V$ variations and (d) the frequency dependence of V_{bi} and N for Ag/Ge/SeO$_2$/Ag MOS devices.

On the other hand, the capacitance and conductance (G) spectra for the AGSA devices are shown in Fig. 5 (a) and (b), respectively. Both C and G parameters are measured under reverse biasing voltage excitations in the range of 0-3.0 V. Imposing signals of low amplitudes ($V = 0.0$ - 0.10 V) the capacitance spectra, in the frequency range of 20-50 MHz, show a peak of negative capacitance (NC) indicating the antiparallel resonance at critical frequency values of 44 MHz. The capacitance spectra then show a resonance at 56 MHz. Negative capacitance effect is a novel property that can be employed for signal amplification, noise reduction and parasitic capacitance cancellation. In addition, negative capacitance effect results in increased gate capacitance leading to enhanced gate controllability and improved switching characteristics [20].

NC formation is believed causing electron-hole recombination by localized traps [21].

It is also evident from Fig. 5 (a) that raising the basing voltage from near zero value to -1.0 V and -2.0 V reduces the negativity of the capacitance and increases the positive part of capacitance. In other words, the resonance in the capacitance becomes more pronounced than the antiresonance. The enhanced resonance in capacitance is accompanied with shift in the critical frequency at which resonance takes place. The resonance frequency increases from 56 MHz to 127 MHz and 163 MHz (inset of Fig. 5 (a)) as the applied voltage increases from 0.0 to -1.0 and -2.0 V, respectively. Further increase in the applied voltage did not shift the critical frequency value but decreases the amplitude of the observed peaks and make the peak of negative capacitance more pronounced. It is mentioned that the negative capacitance dependencies on the bias voltage are assigned to the molecular recombination. In these types of recombination the electrons-holes recombination is mediated by trap states or impurities in materials [21]. The ability of controlling the capacitance dynamics by biasing voltage is an advantage of the AGSA MOS transistors as it allows using it as voltage controlled oscillators [22, 23]. Similar behavior of the AGSA devices was also observed for n-Si/p-CdO transistors [23]. Although n-Si/p-CdO transistors did not show NC effect, they displayed wide controllability of the positive capacitance and conductance in the frequency domain of 20-1000 MHz. Such type of devices was nominated as voltage controlled tunable oscillators in addition to its feature as MOS capacitors [23].

Fig. 5 (b) show the conductance spectra as function of biasing voltage. It is clear from the figure that the conductance at $V = 0.0$ V increases with increasing signal frequency displaying a maxima at 330 MHz followed by a sharp decrease and exhibiting negative conductance values in the frequency range of 425 MHz-447 MHz.
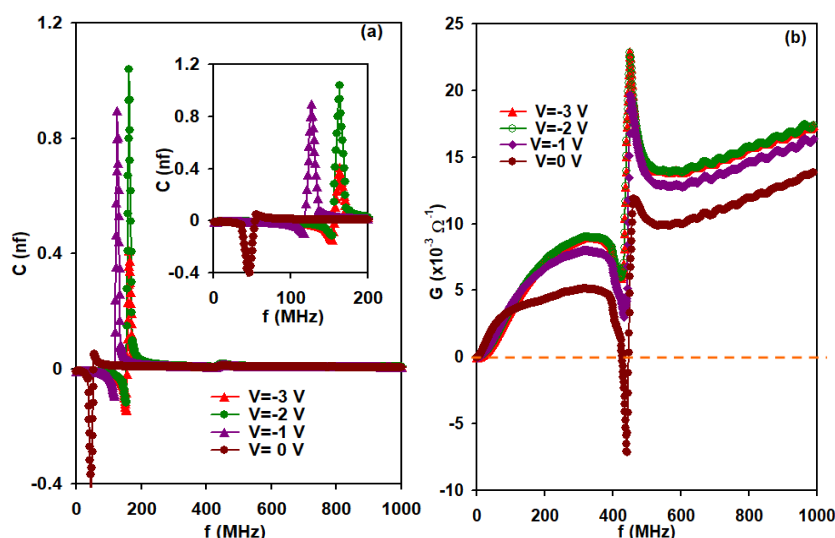
Fig. 5. The voltage controlled (a) capacitance and (b) conductance spectra for Ge/SeO₂ transistors. The inset of (a) showing the shift in C spectra upon basing voltage increase.

Raising the reverse voltage to 1.0 V, 2.0 V, and 3.0 V forces the conductance to exhibit positive values without altering the peaky behavior of the conductance. In other words, the applied

voltage raises the conductance curve up   by increasing the conductance values at each frequency. For examples, at 330 MHz, G increases from 5.1×10^{-3} Ω^{-1} to 8.0×10^{-3} Ω^{-1} and reaches 8.9×10^{-3} Ω^{-1} as the reverse biasing voltage is increased from 0.0 V to 1.0 V and reaches 2.0 V, respectively.   The respective minimum conductance values increases from -7.2×10^{-3} $\Omega^{-1}$to $+3.2 \times 10^{-3}$ Ω^{-1} and reaches $+6.1 \times 10^{-3}$ Ω^{-1}. Negative conductance effect which is found at the gate and source of the device means self-excitation may occur at these frequencies [24]. This feature is significant because it means the ability of using AGSA devices as amplifiers [24]. In hybrid devices, the negative conductance effect is assigned to the tunneling of charge carriers through thin potential barriers that may have formed at the Schottky arms [25].

It is worth notifying that negative conductance and negative capacitance effects were observed in SeO_2 powder pellets pressed at 10.0 MPa [7] and in SeO_2 thin films coated onto Ag substrates. However, $Ag/SeO_2(pellets)/Ag$ and Ag/SeO_2 (thin film) /Ag [6] devices were not sensitive to biasing voltage. MOS characteristics did not appear in these devices. Tuning the negativity of the capacitance and conductance was not possible. The engineering of the conductance and capacitance spectra and the switching from negative resonance to positive resonance in both spectra resulted after using germanium thin crystals as substrates. Hence re-production of the devices onto Ge substrate provided the voltage control facility to the previously reported SeO_2 based electronic devices.   Ge substrates additionally caused the MOS character which can be regarded as novel due to its high frequency responsivity. Compared to recent published data about the high frequency MOS structures like n-type 4H-SiC which succeed in recording C-V characteristic curves up to 100 KHz [26], the currently reported device is of much advanced feature as it performs up to 600 MHz. In addition, compared to $n-Si/p-CdO$ MOS devices which was also responsive up to 700 MHz, the currently reported n-Ge/p-SeO_2 MOS devices [23] show voltage controlled negative conductance and negative capacitance effects.

As an addition information we measured the transfer and output current-voltage characteristics for the transistors under study. The respective current-voltage characteristic curves are shown in Fig. 6 (a) and (b), respectively. It is evident from the figure that standard saturation region is not achievable for the currently studied transistors. This is expected because of the none stoichiometric formation of the p-SeO_2 layer onto n-Ge substrates. Availability of excess anions in the p-layer   make significant contribution to the channel (drain) current and thereby dominates the field effects [27]. In addition, possible interaction between germanium and excess Se may strongly affect the output and transfer characteristic curves of the device understudy. Formation of n-channel in p-layer forces operation in the inverted mode of the transistors when performing as MOS devices. In general, Ge/SeO_2 transistors are more adequate for waveform applications rather than direct current applications. They can perform as novel negative capacitance sources, tunable super capacitors and microwave resonators.
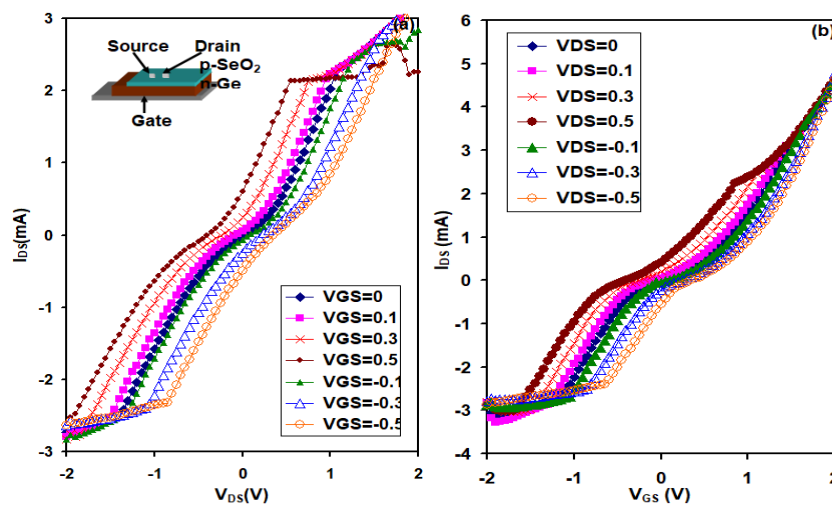
Fig. 6. (a) the transfer and (b) output current-voltage characteristics curves for the Ge/SeO$_2$ thin film transistors.

4. Conclusions

In this work we have shown that SeO_2 layers coated onto Ge thin crystals can perform as metal oxide semiconductor transistors. The transistors exhibit biasing dependent rectification ratios, frequency controlled capacitance voltage- characteristics and voltage controlled capacitance and conductance spectra. The   resonance in the negative capacitance and negative conductance can be tuned via voltage basing. One may switch the amplitude of the negative resonance to positive via reverse biasing of the device. The features of the currently proposed Ge/SeO_2 devices presented by   voltage and frequency controlled negative capacitance, negative conductance, capacitance –voltage characteristics nominate the transistors for use as signal amplifiers, microwave resonators and parasitic capacitance cancellers. The current work is expected to open the doors toward using SeO_2 thin films as promising oxide for electronic applications.

Acknowledgements

References

[1] Sanchez-Perez C, Garcia I and Rey-Stolle I 2022 Fast chemical thinning of germanium wafers for optoelectronic applications Appl. Surf. Sci. 579 152199; https://doi.org/10.1016/j.apsusc.2021.152199

[2] Uddin W, Pasha M S, Dhyani V, Maity S and Das S 2019 Temperature dependent current transport behavior of improved low noise NiGe schottky diodes for low leakage Ge-MOSFET Semicond. Sci. Tech. 34 035026; https://doi.org/10.1088/1361-6641/ab0317

[3] Onik T A M, Hawari H F, Sabri M F M and Wong Y H 2021 Enhancement of electrical performance of Ge-based metal-oxide-semiconductor capacitor via formation of trigonal-Sm2O3 Surf. Interfaces 25 101289; https://doi.org/10.1016/j.surfin.2021.101289

[4] Omotoso E, Paradzah A T, Igumbor E, Taleatu B A, Meyer W E and Auret F D 2020 Determination of capture barrier energy of the E-center in palladium Schottky barrier diodes of antimony-doped germanium by varying the pulse width Mater. Res. Express 7 025901; https://doi.org/10.1088/2053-1591/ab6c1c

[5] Thakur S, Kaur A and Singh L 2019 Mixed valence effect of Se6+ and Zr4+ on structural, thermal, physical, and optical properties of B2O3-Bi2O3-SeO2-ZrO2 glasses Opt. Mater. 96 109338; https://doi.org/10.1016/j.optmat.2019.109338

[6] Alharbi S R, Qasrawi A F and Algarni S E 2022 Growth and characterization of (glass, Ag)/SeO2 thin films Physica B. 633 413790; https://doi.org/10.1016/j.physb.2022.413790

[7] Algarni S E, Qasrawi A F and Khusayfan N M 2022 Hydraulic pressure and temperature effects on the structural, morphological and electrical properties of SeO2 powders Appl. Phys. A. 128 1-11; https://doi.org/10.1007/s00339-022-05392-5

[8] Venimadhav A, Lekshmi I C and Hegde M S 2002 Strain-induced metallic behavior in PrNiO3 epitaxial thin films Mater. Res. Bull. 37 201-208; https://doi.org/10.1016/S0025-5408(01)00777-2

[9] Chaudhary P, Shukla R, Dabas S and Thakur O P 2021 Enhancement of structural, magnetic, dielectric, and transport properties of Nb substituted 0.7BiFeO3-0.3 BaTiO3 solid solution J. Alloy. Compd. 869 159228; https://doi.org/10.1016/j.jallcom.2021.159228

[10] Wang L, Li J J, Fan Q, Huang Z F, Lu Y C, Xie C, Wu C Y and Luo L B 2019 A high-performance near-infrared light photovoltaic detector based on a multilayered PtSe2/Ge heterojunction J. Mater. Chem. C. 7 5019-5027; https://doi.org/10.1039/C9TC00797K

[11] Sze S M, Li Y and Ng K K 2021 Physics of semiconductor devices (John wiley & sons)

[12] Khusayfan N M, Qasrawi A F and Khanfar H K 2018 Design and electrical performance of CdS/Sb2Te3 tunneling heterojunction devices Mater. Res. Express 5 026303; https://doi.org/10.1088/2053-1591/aaadda

[13] Zhang J, Xu J, Yang L, Cao Z, Yuan C, Zhou C, Wang H and Rao G 2022 Controlling light-induced dielectric response of Sr/Ni-modified (K0.5Na0. 5) NbO3 ceramics by narrow bandgap method Mat. Sci. Semicon. Proc. 143 106521; https://doi.org/10.1016/j.mssp.2022.106521

[14] Chin A, Kao H L, Tseng Y Y, Yu D S, Chen C C, McAlister S P and Chi C C 2005 Physics and modeling of Ge-on-insulator MOSFETs In Proceedings of 35th European Solid-State Device Research Conference 285-288 (IEEE)

[15] Nakashima S, Fujisawa H, Suminaga H, Park J M, Nishioka H, Kobune M, Kanashima T, Okuyama M and Shimizu M 2011 Preparation of BiFeO3 thin films on SrRuO3/SrTiO3 (001) substrate by dual ion beam sputtering Jpn. J. Appl. Phys. 50 09NB01; https://doi.org/10.1143/JJAP.50.09NB01

[16] Qasrawi A F2020 Characterization of Au/As2Se3 multifunctional tunneling devices phys. status solidi (a) 217 1900899; https://doi.org/10.1002/pssa.201900899

[17] Qasrawi A F, Khanfar H K and Alyat S B 2022 Design and Characterization of Yb/ p-p-SiO2/(Yb, In) Thin-film Transistors for 5G Resonators Braz. J. Phys. 52 1-7; https://doi.org/10.1007/s13538-022-01058-y

[18] Madelung O 2004 Semiconductors: data handbook (Springer Science & Business Media); https://doi.org/10.1007/978-3-642-18865-7

[19] Khusayfan N M, Khanfar H K and Alharbi S R 2021 Design and Characterization of Au/CdSe/GeO2/C MOSFET Devices Mater. Res. 24; https://doi.org/10.1590/1980-5373-MR-2021-0020

[20] Bansal M and Kaur H 2018 Performance investigation of Negative Capacitance Germanium Double Gate-pFET (NCGe-DG-pFET) for improved analog applications In 2018 International Symposium on Devices, Circuits and Systems (ISDCS) 1-4 (IEEE); https://doi.org/10.1109/ISDCS.2018.8379686

[21] KARATAŞ Ş 2021 Temperature and voltage dependence C-V and G/ω-V characteristics in Au/n-type GaAs metal-semiconductor structures and the source of negative capacitance J. Mater. Sci. 32 707-716; https://doi.org/10.1007/s10854-020-04850-1

[22] Choudhuri B and Mummaneni K 2022 A Review on a Negative Capacitance Field-Effect Transistor for Low-Power Applications J. Electron. Mater. 51 1-15; https://doi.org/10.1007/s11664-021-09384-8

[23] Harbi S R A and Qasrawi A F 2021 Design and characterization of n-Si/p-CdO broken gap heterojunctions as high frequency PMOSFETs and microwave resonators IEEE Sens. J. 21 13223-13229; https://doi.org/10.1109/JSEN.2021.3065681

[24] Wu T and Wu J 2021 AL band Power Amplifier Design with RC Stability Network. In 2021 International Conference on Microwave and Millimeter Wave Technology (ICMMT) 1-3 (IEEE); https://doi.org/10.1109/ICMMT52847.2021.9618244

[25] Qasrawi A F and Aloushi H D 2019 Formation, negative capacitance and negative conductance effects in Selenium stacked layers sandwiched with Ag nanosheets Mater. Res. Express 6 086435; https://doi.org/10.1088/2053-1591/ab2083

[26] Guo Z, Wu J, Tian R, Wang F, Xu P, Yang X and He Z 2021 Extraction of the Trench Sidewall Capacitances in an n-Type 4H-SiC Trench Metal-Oxide-Semiconductor Structure IEEE T. Electron Dev. 68 2879-2885; https://doi.org/10.1109/TED.2021.3075168

[27] Saxena V, Chauhan AK, Padma N, Aswal DK, Koiry SP, Sen S, Tokas RB, Gupta SK, Sürgers C and Yakhmi JV 2009 Poly (3-hexylthiophene) based field-effect transistors with gate SiO2 dielectric modified by multi-layers of 3-aminopropyltrimethoxysilane. Thin Solid Films. 517 6124-8; https://doi.org/10.1016/j.tsf.2009.05.031